Plasma Energy Transfer to Metal Surfaces Irradiated by Pulsed Lasers

A. N. Pirri,* R. G. Root,* and P. K. S. Wu*
Physical Sciences Inc., Woburn, Mass.

Recent experimental data have indicated that when highly reflective metal targets are irradiated by pulsed lasers in an air environment, a larger fraction of the incident laser energy is coupled into the target when a plasma is ignited above the surface than when plasma formation does not occur. Models of the plasmadynamics and subsequent energy transfer to the surface by radiation and conduction are constructed in order to predict the thermal coupling coefficient (coupled energy/laser energy) for pulsed laser irradiation of a metal target. It is found that the largest fraction of the incident laser energy is coupled into the target when a laser-supported combustion wave is ignited in close proximity to the surface. Energy transfer is via reradiation from the absorbing air plasma. Techniques for obtaining maximum thermal coupling are suggested as a result of the theoretical models. Results are compared with both computer simulations of the plasmadynamics and existing experimental data.

I. Introduction

WHEN a pulsed laser beam irradiates a metal target, the fraction of the incident energy that is coupled into the target is usually represented by the intrinsic absorptivity of the metal. However, recent experiments with highly reflective metals have shown that at high laser intensities this fraction is substantially greater than the absorptivity of the target material.[1] This so-called "enhanced thermal coupling" is observed simultaneously with the onset of plasma formation above the surface. Therefore, it is concluded that the increase in the coupled energy is a result of energy transfer from the plasma that is significantly larger than energy transfer from direct infrared laser radiation on the target surface. The purposes of this paper are to 1) present simplified models for the plasma configuration generated by pulsed laser irradiation of highly reflective targets, 2) evaluate the potential of radiation and conduction energy transfer mechanisms as a result of plasma formation, and 3) deduce under what conditions the fraction of laser energy coupled to the target material is maximum.

The dynamics of a laser-produced plasma above a surface will depend upon the intensity of the incident laser pulse and the pulse duration. At laser intensities slightly greater than the plasma threshold intensity, a laser-supported combustion (LSC) wave[2] is usually ignited. LSC waves are often seen at intensities from 2×10^4 W/cm^2-10^6 W/cm^2 for 10.6 μm radiation with both pulsed and CW laser beams. The ignition of an LSC wave initially takes place in the target vapor.[3,4] The heated target vapor subsequently transfers its energy to the surrounding air. Once the air begins to absorb a significant fraction of the laser energy, the LSC wave propagates into the air along the beam path. When the laser pulse is too short to initiate bulk evaporation of the target surface, ignition may result from vaporization of flakes or imperfections on the surface and subsequent breakdown of vapor pockets.[5,6] Nonetheless, the result is an LSC wave that propagates into the air above the target. As a consequence of the ignition process and the presence of the target surface, a precursor shock precedes the LSC wave, except at the lowest intensities. When the LSC wave has propagated far enough for two-dimensional effects to dominate the plasma flow in the vicinity of the surface, the plasma configuration resembles that shown schematically in Fig. 1a. The LSC wave propagating into the air behind the precursor shock induces a flow toward the target. Close to the surface the flow resembles a stagnation point flow. A stagnation point boundary-layer analysis must be matched to a correct model for the LSC wave propagating away from the surface in order to obtain the temperature and pressure distribution in the plasma, the radiative transport to the target, and the conductive energy transfer.

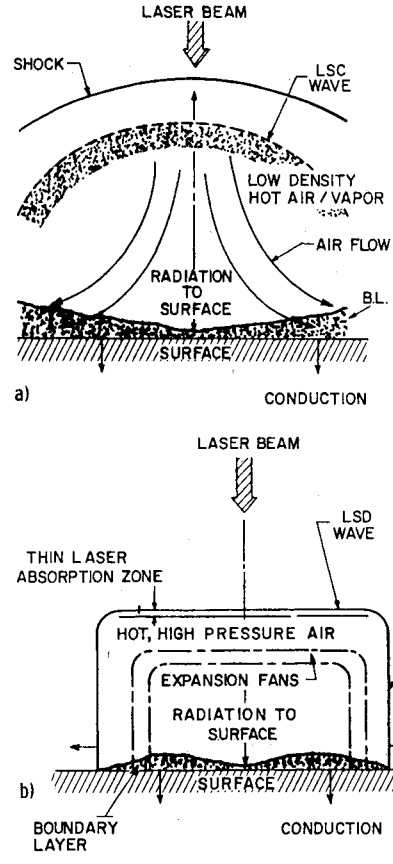

Fig. 1 a) LSC wave plasmadynamics; b) LSD wave plasmadynamics.

Presented as Paper 77-658 at the AIAA 10th Fluid and Plasmadynamics Conference, Albuquerque, N. Mex., June 27-29, 1977; submitted Aug. 5, 1977; revision received July 5, 1978.

Index categories: Lasers; Radiatively Coupled Flows and Heat Transfer; Radiation and Radiative Heat Transfer.
*Principal Scientist. Member AIAA.

At higher laser intensities ($>10^7$ W/cm^2 for 10.6 μm laser radiation), a laser-supported detonation (LSD) wave[7] is ignited. The mechanism for igniting these waves above surfaces is not completely understood, but it is believed that ignition takes place rapidly off surface protrusions that vaporize and break down.[6] A simplified model of the plasma configuration resulting from LSD wave ignition is shown in Fig. 1b. The laser beam absorption takes place in a thin zone of hot, high-pressure air behind the detonation wave. Since the detonation wave drags air away from the surface, expansion fans form to satisfy the boundary condition of zero particle velocity at the target surface. One-dimensional gasdynamics can be matched to detonation and planar blast wave theory to describe this aspect of the flowfield, and cylindrical blast-wave theory can be utilized to partially account for two-dimensional effects.[8] An unsteady boundary layer forms on the surface; it resembles the boundary layer behind a propagating shock wave as the cylindrical blast wave spreads out over the target. Energy is transferred from the plasma to the target through this boundary layer by radiation and conduction.

Enhanced thermal coupling is synonymous with the onset of plasma formation and the level of the "enhancement" decreases as the laser intensity increases. The decreased level of the "enhancement" is a result of transition from an LSC wave plasma to an LSD wave plasma. Therefore, in order to understand thermal coupling mechanisms and how they scale with laser parameters, it is necessary to model how this transition takes place. The transition at 10.6 μm occurs between 10^6 and 10^7 W/cm^2. This will be discussed later, but first the energy transfer to the target from the LSC wave plasma will be presented in Sec. II. Transition from an LSC wave to an LSD wave is discussed in Sec. III, and implications with regard to laser conditions for maximum thermal coupling are presented in Sec. IV. Correlations of existing data and comparison with theory is discussed in Sec. V and conclusions are presented in Sec. VI.

II. Energy Transfer from an LSC Wave Plasma

The energy transfer from an LSC wave plasma can be best examined if the configuration is treated initially as one-dimensional. A schematic of this idealization is presented in Fig. 2. Throughout the analysis it is assumed that the plasma is an air plasma. This configuration has been studied theoretically by previous investigators and a summary of their contributions is presented in Ref. 3. The precursor shock propagates into the surrounding air; the LSC wave defines the leading edge of the absorbing plasma and proceeds into the shocked air by radiative energy transport. The velocity at which the LSC wave propagates into the shocked gas along with the shock strength will determine the plasma properties and the strength of the energy transferred to the target from the plasma. The problem is unsteady because, in general, the LSC wave and the shock have different absolute velocities. An approximate solution, when the LSC wave velocity approaches the shock velocity, will be discussed later. However, a quasisteady solution can be obtained for a simplified configuration where the properties are considered uniform between the shock and the LSC wave and between the LSC wave and the wall. The gasdynamic relations, which govern the motion of the shock and LSC wave plasma, as configured in Fig. 2 can be best described by considering the gas within the expanding volume denoted by the dashed line. One boundary of this volume is attached to the LSC wave and the other is fixed to the wall. With reference to the LSC wave, the boundary moves at the absolute LSC wave velocity V_w. Therefore, conservation of energy within this volume becomes:

$$\frac{d}{dt}\left[\rho\left(h+\frac{V^2}{2}\right)L\right]=\rho_s(V_w-u_s)\left[h_s+\frac{(V_w-u_s)^2}{2}\right]+I_0-q_r-q_\ell \tag{1}$$

where ρ and h are the density and enthalpy, respectively, in the plasma between the LSC wave and the wall; V is the particle velocity with reference to the coordinate system attached to the LSC wave; L is the distance between the LSC wave and the wall; ρ_s is the density between the shock and the LSC wave; u_s is the particle velocity behind the shock, measured in a wall fixed coordinate system; h_s is the enthalpy behind the shock; I_0 is the incident laser intensity, q_r is the radiation lost from the plasma to the wall; and q_ℓ is the radiation lost upstream through the layer between the shock and the LSC wave. It is assumed that all the laser energy is absorbed by the plasma and that conduction losses only affect a region very close to the surface. Therefore, conduction is neglected in the overall energy balance of Eq. (1). If the LSC wave is treated as a discontinuity and the conditions are taken to be uniform throughout the plasma, Eq. (1) reduces to:

$$\rho V_w\left(h+\frac{V_w^2}{2}\right)=\rho_s(V_w-u_s)\left[h_s+\frac{(V_w-u_s)^2}{2}\right]+I_0-q_r-q_\ell \tag{2}$$

Similarly, the equations of mass and momentum across the LSC wave in terms of the coordinate system attached to the LSC wave become

$$\rho V_w=\rho_s(V_w-u_s) \tag{3}$$

$$p+\rho V_w^2=p_s+\rho_s(V_w-u_s)^2 \tag{4}$$

where p_s is the pressure behind the shock and p is the pressure in the plasma. q_ℓ is the low-frequency radiation that is lost through the wave front and will be treated as a negligible fraction of the laser intensity. A perfect gas equation of state is used in each region with different values of the effective heat ratio. Therefore, in the plasma the relation between pressure, density, and enthalpy can be written

$$p=\frac{(\gamma-1)}{\gamma}\rho h \tag{5}$$

where γ is taken to be 1.2 in the air plasma. Across the shock wave, strong shock relations yield

$$V_s=\frac{\gamma_s+1}{2}u_s \tag{6}$$

$$p_s=\frac{\gamma_s+1}{2}\rho_\infty u_s^2 \tag{7}$$

$$\rho_s=\frac{\gamma_s+1}{\gamma_s-1}\rho_\infty \tag{8}$$

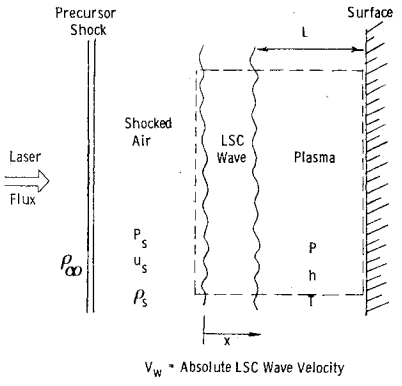

Fig. 2 Laser supported combustion wave plasma in one dimension.

where V_s is the shock velocity, γ_s is the specific heat ratio between the shock and the LSC wave (taken to be 1.4), and ρ_∞ is the ambient density.

It has been demonstrated by Thomas[3] that relations similar to Eqs. (1-8) can be manipulated to determine the plasma conditions in terms of the absorbed laser intensity and the particle velocity through the LSC wave. The shock pressure, particle velocity, plasma pressure, and plasma enthalpy become

$$p_s = \left[\frac{\gamma_s + 1}{2}\rho_\infty\right]^{1/3}\left[\frac{(\gamma-1)(\gamma_s-1)I_p}{(\gamma+W)(\gamma_s-1-2W)}\right]^{2/3} \tag{9}$$

$$u_s = \left[\frac{2(\gamma-1)(\gamma_s-1)I_p}{(\gamma_s+1)\rho_\infty(\gamma+W)(\gamma_s-1-2W)}\right]^{1/3} \tag{10}$$

$$p/p_s = 1-2W/(\gamma_s-1) \tag{11}$$

$$h/u_s^2 = \gamma(1+W)(\gamma_s-1-2W)/2(\gamma-1)W \tag{12}$$

where $I_p = I_0 - q_r - q_\ell$ and W is the nondimensionalized particle velocity through the LSC wave defined as $W = (V_w - u_s)/u_s$. The only difference between Eqs. (9-12) and the relations in Ref. 3 is the inclusion of the radiation loss to the wall in the definition of I_p. It will be shown in Sec. III that the transition from LSC to LSD wave plasmadynamics can be described using Eqs. (9-12). However, for the present, it can be seen that this system of equations cannot be closed until the radiative transport relations for the LSC wave propagation are included (to determine V_w). Thomas has obtained approximate solutions in the limit of small W by replacing the transport relations that describe the LSC wave propagation by a radiative equilibrium assumption. This assumption plus appropriate thermodynamic relations close the system of equations so that the plasma properties and the particle velocity through the LSC wave can be calculated. This radiative equilibrium assumption implies that one half of the absorbed laser energy is radiated toward the target. If all of the energy is absorbed by the target surface, the thermal coupling coefficient (q_r/I_0) is 50%.

When $W \to 0$, the LSC wave velocity approaches the particle velocity behind the shock. It will be shown later that the radiative equilibrium approximation is only valid for $W \ll 1$. The actual motion of the LSC wave in the preshocked gas can only be determined if a detailed calculation of the radiation transport within the LSC wave is included. When this calculation is included, it is not necessary to utilize the radiative equilibrium assumption, and the actual thermal coupling coefficient can be computed. Such calculations have been performed in the following way. First, a model for predicting LSC wave velocities and the thermodynamic properties within an LSC wave has been developed and is described in Ref. 9. The model differs from previous LSC wave models[10,11] in that although the radiative transport through the LSC wave is treated in a simplified manner, the effect of laser attenuation is included. The solution is obtained by treating the laser intensity as an eigenvalue and integrating the energy equation (along with the momentum equation) through the LSC wave:

$$\rho_s(V_w-u_s)\left[c_p(T)\frac{dT}{dx} + \left(\frac{\partial h}{\partial p}\right)_T\frac{dp}{dx}\right] + q(T)$$

$$-k_L(T)I_0\exp\left[-\int_0^x k_L(T)\,dx\right] = \frac{d}{dx}\left(\lambda(T)\frac{dT}{dx}\right) \tag{13}$$

where the coordinate system is attached to the leading edge of the LSC wave and x is positive toward the surface (see Fig. 2), ρ_s is the density behind the precursor shock, T is the temperature, c_p is the specific heat at constant pressure, $q(T)$ is the radiative loss, $k_L(T)$ is the effective absorption coefficient for the laser radiation, I_0 is the incident laser intensity, and $\lambda(T)$ is the combined thermal and radiative conductivity. Because of the nature of Eq. (13), the calculated profile of the temperature through the LSC wave will correspond to the true profile only if the selected eigenvalue I_0 is the correct intensity for the corresponding mass flow through the LSC wave, $\rho_s(V_w - u_s)$. If I_0 is greater than the correct intensity, the temperature profile rapidly decreases toward zero temperature as you integrate through the LSC wave. If I_0 is less than the correct intensity, the temperature continually increases rapidly. Only when I_0 is within 0.01% of the correct intensity (for the corresponding mass flow) will the solution be self-consistent. This extreme sensitivity to the eigenvalue enables a solution to be obtained with only a few iterations.[9]

Utilizing the preceding technique to obtain the mass flow through the LSC wave (and thus, W), we can calculate the resulting plasma properties as a function of laser intensity and time for 10.6 μm laser radiation. The numerical solutions are actually obtained in an inverse manner. The pressure behind the precursor shock is assumed for a specific intensity I_0. From integration of Eq. (13), W is obtained. Substituting into Eq. (9), we then can calculate I_p. When q_ℓ is neglected, q_r is obtained from the expression $I_p = I_0 - q_r$. If the plasma is considered to be a uniform temperature slab, the radiation flux into the surface can be written

$$q_r = \epsilon\sigma T^4 \tag{14}$$

where $\epsilon(L,\rho,T)$ is the total slab emissivity and $\sigma = 1.03\times10^5$ W/cm^2 – (eV)^4 is the Stefan-Boltzmann constant. Curve-fitting the results of Johnston et al.,[12] we obtain the following expression over the range of interest

$$\epsilon = 1.02T^{2.2}L^{0.36}(\rho/\rho_\infty) \quad \text{for } 1.5 \text{ eV} \le T \le 2 \text{ eV} \tag{15a}$$

$$\epsilon = 0.31T^{5.3}L^{0.43}(\rho/\rho_\infty) \quad \text{for } 1.2 \text{ eV} \le T \le 1.5 \text{ eV} \tag{15b}$$

The thickness of the slab is $L = V_w t$ where t is time since plasma formation. The remaining plasma properties are calculated from Eqs. (10-12); the curve fit of Gilmore[13] is used to relate internal energy to temperature and density, and $h = \gamma e = [\gamma/(\gamma-1)]p/\rho$ is used to close the system. Therefore, for each I_0 and ρ_s there is a unique q_r, L, and t. As a function of I_0 and time t we can obtain all the plasma properties. Example results for p and T as a function of laser intensity and time are presented in Figs. 3 and 4. These results are valid until $\epsilon = 1$ (i.e., the plasma becomes black), after which the plasma conditions remain constant. One result of these calculations is that below 10^7 W/cm^2 the relative velocity of the LSC wave in the preshocked air ($V_w - u_s$) is sufficiently small that $W \to 0$ is a good approximation for determining the pressure, shock strength, and particle velocity behind the shock. As you increase the intensity, W increase as transition from the LSC to LSD wave dynamics occurs. A discussion of the phenomenology of LSC/LSD wave transition will be presented in Sec. III.

Once the plasma properties have been specified, the energy transfer to the target by conduction and radiation can be estimated. Throughout the analysis it has been assumed that the plasma is an air plasma. Some investigators have indicated that the vapor may play a significant role in the energy transfer to the target.[5,14] At wavelengths shorter than 10.6 μm and ambient pressures less than 1 atm, the vapor effects would be expected to increase. At 1 atm and 10.6 μm, it is only possible to determine the amount of vapor present if the surface uniformly vaporizes. However, at intensities $\approx 10^6$ W/cm^2 with laser pulse times $\approx$ 10-30 μs, the surface will not reach the vaporization temperature and vapor is produced by evaporating flakes or surface protrusions.[3] The amount of vapor will then depend upon surface preparation and the vapor density will be very difficult to calculate. Throughout the remainder of this paper the plasma will be considered to

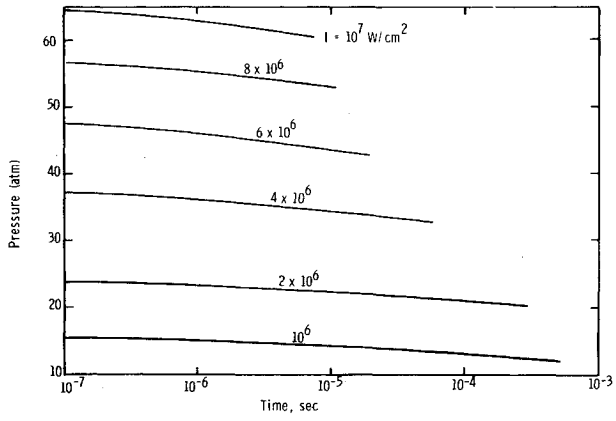

Fig. 3 Plasma pressure vs time.

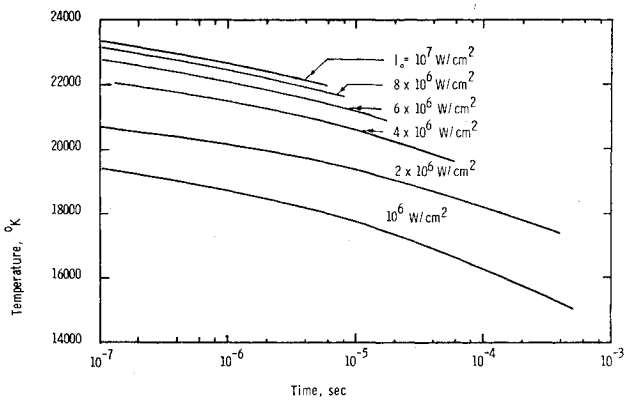

Fig. 4 Plasma temperature vs time.

be air and the energy transfer from the air plasma to the target will be determined. More comments regarding the role of target vapor will be made in Sec. V.

Energy Transfer by Thermal Conduction

Energy transfer by conduction takes place through the boundary layer. It is anticipated that three boundary-layer configurations must be considered. During an early time, a one-dimensional thermal boundary layer is formed between the plasma and the cold wall. Once two-dimensional effects begin to dominate the plasma configuration, the boundary layer resembles the boundary layer behind a shock propagating along a wall. Finally, at a later time, when the flow along the axis of symmetry reverses and acquires a velocity component toward the wall, a stagnation point boundary-layer profile becomes more appropriate in the vicinity of the center of the laser spot.

The boundary-layer analyses necessary to determine quantitatively the energy transfer to the surface by conduction are carried out in detail in Refs. 9 and 15. It was found using a one-dimensional, boundary-layer analysis that, when the plasma is at 10-100 atm and 1-2 eV in temperature, the conductive energy transfer $q_w\sqrt{t}$, where q_w is the heat transfer in W/cm^2 and t is the time since plasma formation, ranges from 15 to 120 (W/cm^2) s$^{1/2}$. For times up to 100 μs, the integrated heat transfer by this mechanism is much too small to transfer greater than 3% of the laser energy. Therefore, conductive heat transfer in the one-dimensional geometry is too small to explain enhanced thermal coupling.

Energy Transfer by Radiation

The radiation emitted from a plasma slab was obtained in detail by Wilson and Greif[16] and can also be computed from Eq. (14). Wilson and Greif calculated in detail the power radiated from an isothermal air plasma slab as a function of

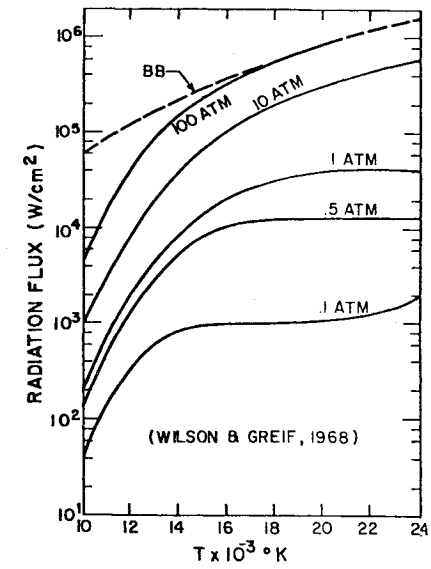

Fig. 5 Wilson and Greif[16] result for radiation from 3-cm thick plasma slab.

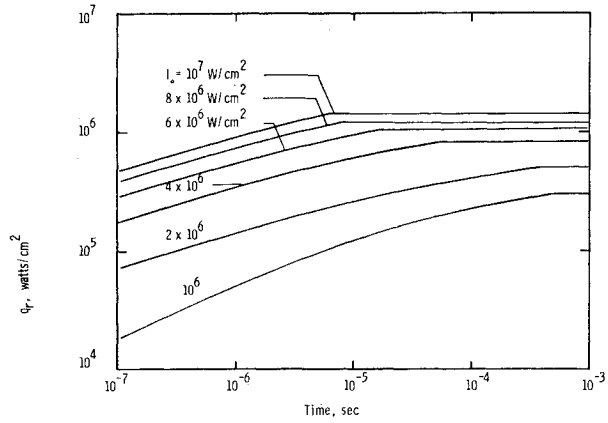

Fig. 6 Radiation flux to surface vs time.

temperature, pressure, and slab thickness. An example result is presented in Fig. 5 for a slab thickness $\delta = 3$ cm (BB denotes the black body limit). It can be seen immediately that for a slab thickness of 3 cm, more than 10^5 W/cm^2 will be radiated to the surface from the plasma when the plasma temperature is greater than 16,000 K and the pressure is greater than 10 atm. In addition, results for the radiation flux to the surface, obtained from Eqs. (14) and (15) and Figs. 3 and 4, are shown in Fig. 6. It can be seen that for late times (>10 μs), greater than 10% of the incident laser intensity is radiated toward the surface. The spectral content of the reradiated energy is such that the VUV (<2000 Å) dominates when pressures are ≈ 1 atm. At higher pressures, the visible and IR continuum begin to contribute significantly. An example calculation[16] at 10 atm for $\delta = 30$ cm shows 50% is in the visible and IR continuum. The actual energy absorbed by the target cannot be determined until the spectral absorption properties of the surface are included; however, the preceding calculations indicate that a thermal coupling coefficient (ratio of energy coupled into target to laser energy) greater than the intrinsic 3% absorptivity of the aluminum surface to 10.6 μm radiation is realistic. The actual coupling coefficient calculations are outlined in the next subsection. However, the dominant energy transfer mechanism in this plasma regime is radiation.

Coupling Coefficient Calculations

The effectiveness of removing material with a high-power laser depends upon the energy/area that is coupled into the surface. Therefore, it is appropriate to define the thermal coupling coefficient as:

$$\alpha = \int q_r \, dt / \int I_0 \, dt \qquad (16)$$

where q_r is the radiation flux to the surface at any point on the surface. For the present it will be assumed that the laser beam has a uniform spatial distribution of intensity out to the edge of the spot. Therefore, the maximum value of α over the spot area occurs on the beam centerline. This value of α will be denoted as the "central" coupling coefficient.

In the one-dimensional regime the behavior of α as a function of time can be computed by using the results of Fig. 6. From Fig. 6 it can be seen that the radiation flux to the surface increases with time until the plasma becomes black; for longer times the radiation flux to the surface becomes constant. If we curve fit these results such that

$$q_r \approx A_p t^m \tag{17}$$

simple expressions for the coupling coefficient as a function of time can be derived. For the present it will be assumed that all the radiation flux deposited onto the surface is absorbed. Modification to account for the spectral absorption coefficient of the surface will be discussed later. Two-dimensional effects begin to decrease the pressure and temperature in the plasma (and thus the radiation q_r) when expansion fans from the edges of the spot reach the centerline. This time scale is approximately the spot radius divided by the sound speed in the plasma. Therefore, a one-dimensional coupling coefficient can only be calculated over time scales.

$$t \le \tau_{2D} = R_s / a_p \tag{18}$$

where R_s is the spot radius and a_p is the sound speed calculated at the plasma temperature. Using Eq. (18) for pulse times, τ_p, greater than a time t that satisfies Eq. (18), we obtain for the coupling coefficient

$$\alpha = \frac{\int_0^t q_r \mathrm{d}t}{\int_0^t I_0 \mathrm{d}t} = \frac{A_p {\tau_{2D}}^m}{(m+1) I_0} \left(\frac{t}{\tau_{2D}}\right)^m \quad (t < \tau_{2D}) \tag{19}$$

When the laser pulse terminates, radiation from the plasma will contine to reach the surface while the plasma cools. In order to compute the coupling coefficient after the pulse ends, the dynamics of the cooling process must be modeled. In Ref. 8, blast wave scaling laws were used to model the decay of the laser-supported detonation wave (after pulse termination) and the cylindrical shock wave that traverses the surface after the plasma becomes two-dimensional. With the LSC wave plasma configuration of Figs. 1a and 2 the precursor shock, and thus the plasma pressure and velocity, will be assumed to decay as predicted by blast wave scaling. The remaining plasma properties will be computed by assuming that the hot plasma behind the precursor shock decays isentropically. The blast wave scaling will be utilized as follows:

For $\tau_p < t < \tau_{2D}$:

$$L \approx L_p (t/\tau_p)^{2/3}, \quad p \approx p_p (\tau_p / t)^{2/3} \tag{20}$$

For $\tau_{2D} < \tau_p < t$:

$$L \approx L_p (t/\tau_p)^{2/5}, \quad p \approx p_p (\tau_p / t)^{6/5} \tag{21}$$

For $\tau_{2D} < t < \tau_p$:

$$L \approx L_{2D} (t/\tau_{2D})^{3/5}, \quad p = p_{2D} (\tau_{2D} / t)^{4/5} \tag{22}$$

where L_p and p_p are the plasma thickness and pressure, respectively, at the pulse time τ_p, and L_{2D} and p_{2D} are the thickness and pressure, respectively, at the two-dimensional time τ_{2D}. Equation (20) is the one-dimensional blast wave decay scaling, Eq. (21) is the spherical blast wave decay scaling, and Eq. (22) is the spherical blast wave decay scaling for linear increase in energy with time. The change in plasma density as the pressure decays is found by assuming that the plasma decays isentropically, i.e., $p/\rho^\gamma = \text{const}$. The temperature follows from the equation of state. Using Eqs. (14-17), (19), and (20-22) $p/\rho^\gamma = \text{const}$. and the equation of state of Gilmore,[13] we can construct expressions for α as a function of time in both one- and two-dimensional regimes. After much algebra, we obtain the following results:

For $\tau_p < \tau_{2D}$:

$$\alpha(t) = \frac{A_p \tau_p^m}{(m+1) I_0} \left(\frac{t}{\tau_p}\right)^m \quad (t < \tau_p) \tag{23}$$

$$\alpha(t) = \frac{A_p \tau_p^m}{I_0} \left\{ \frac{1}{(m+1)} + 6.6 \left[1 - \left(\frac{\tau_p}{t}\right)^{0.15} \right] \right\} \quad (\tau_p \le t \le \tau_{2D}) \tag{24}$$

$$\alpha(t) = \frac{A_p \tau_p^m}{I_0} \left\{ \frac{1}{(m+1)} + 6.6[1 - \hat{\tau}^{0.15}] + 0.645 \hat{\tau}^{0.15} \left[1 - \left(\frac{\tau_{2D}}{t}\right)^{1.55} \right] \right\} \quad (t > \tau_{2D}) \tag{25}$$

where $\hat{\tau} = \tau_p / \tau_{2D}$.

For $\tau_p > \tau_{2D}$:

$$\alpha(t) = \frac{A_p \tau_p^m}{(m+1) I_0} \left(\frac{t}{\tau_p}\right)^m \quad (t < \tau_{2D}) \tag{26}$$

$$\alpha(t) = \frac{A_p {\tau_{2D}}^{m+1}}{I_0} \left\{ \frac{1}{(m+1) t} + \frac{2}{t} \left[1 - \left(\frac{\tau_{2D}}{t}\right)^{.5} \right] \right\} \quad (\tau_{2D} \le t \le \tau_p) \tag{27}$$

$$\alpha(t) = \frac{A_p \tau_{2D}^m}{I_0} \left\{ \frac{1}{(m+1)\hat{\tau}} + \frac{2}{\hat{\tau}} \left[1 - \left(\frac{1}{\hat{\tau}}\right)^{.5} \right] + \frac{.645}{\hat{\tau}^{1.5}} \left[1 - \left(\frac{\tau_p}{t}\right)^{1.55} \right] \right\} \quad (t > \tau_p) \tag{28}$$

The final value of the coupling coefficient is obtained by setting $t = \infty$ in either Eq. (25) or (28); Eq. (25) is used for $\tau_p < \tau_{2D}$ while Eq. (28) is for $\tau_p > \tau_{2D}$.

The features of a coupling coefficient vs time calculation are presented in Fig. 7. The true value of the coupling coefficient will depend upon the fraction of the radiation flux impinging on the surface that is actually absorbed. Therefore, the spectral absorption coefficient of the surface must be included in any calculation. Aluminum has a high reflectivity in the infrared, but its reflectivity decreases dramatically in the visible and ultraviolet. Unfortunately, data for the spectral absorptance of aluminum at elevated temperature are sparce. Recently, Boni et al.[17] presented a two-dimensional computer code simulation of the plasma formation above an aluminum target irradiated by a pulsed laser. For simplicity, Boni assumed that all radiation impinging upon the surface at wavelenths <1100 Å is absorbed, while only 50% of the radiation at wavelengths ≥ 1100 Å is absorbed. Since it is desirable to compare the results of our simplified model with Boni's computer code, the same assumption will be used. Therefore,

$$q_{r_{abs}} = q_{r_{\lambda < 1100\text{Å}}} + 0.5 q_{r_{\lambda > 1100\text{Å}}} \tag{29}$$

As a further simplification, it will be assumed that the fraction of the incident radiation flux to the surface that is

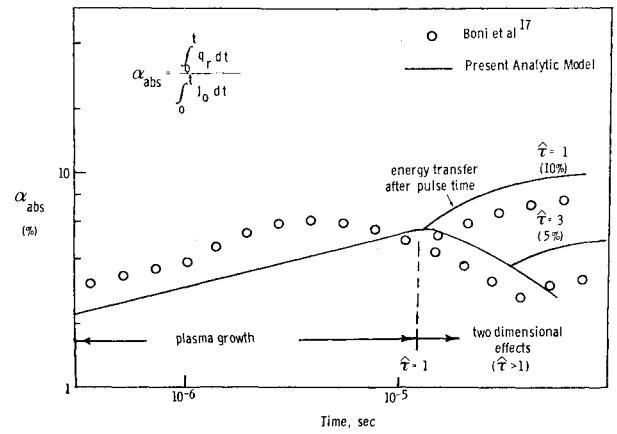

Fig. 7 Central coupling coefficient vs time; $A_s = 113$ cm^2; $I_0 = 5 \times 10^6$ W/cm^2.

absorbed remains constant throughout the development and decay of the plasma. Therefore, we shall write $\alpha_{abs} = \beta\alpha$ where the fraction β will be computed from the spectral content of the radiation flux to the surface in the one-dimensional regime. q_r as a function of temperature and pressure can be determined from Figs. 3, 4, and 6. The radiation flux at < 1100 Å is black body. Therefore, the flux in this wavelength regime can be obtained simply by integrating the Planck function over wavelengths from 0 to 1100 Å. Subtracting from q_r gives the contribution from $\lambda > 1100$ Å.

Using the preceding technique, we obtain $\beta \approx 0.7$, 0.6, 0.55 for $I_0 = 10^6$ W/cm^2, 4×10^6 W/cm^2, and 10^7 W/cm^2, respectively. The fraction decreases with increasing intensity because at higher pressures the spectral content shifts toward the visible and infrared. Also, for calculations at representative intensities the constants in Eq. (17) are as follows when t is in seconds and q_r is in Watts per cm^2: $A_p \approx 6.8 \times 10^6$ and $m \approx 0.35$ at $I_0 = 10^6$ W/cm^2, $A_p \approx 4.8 \times 10^6$ and $m \approx 0.25$ at $I_0 = 2 \times 10^6$ W/cm^2, $A_p \approx 1.06 \times 10^7$ and $m \approx 0.25$ for $I_0 = 4 \times 10^6$ W/cm^2. Results for α_{abs} vs t with an intensity of 5×10^6 W/cm^2 and spot area of 113 cm^2 are shown in Fig. 7. Early on, the coupling coefficient increases, since the plasma becomes more opaque as it grows and radiates a larger fraction of the incident laser intensity. At $t = 12$ μs, $\hat{\tau} = 1$. If the pulse terminates at this point, the coupling coefficient continues to increase since the plasma continues to radiate as it cools. If the pulse duration is greater than τ_{2D} (i.e., $\hat{\tau} = \tau_p/\tau_{2D} > 1$), the coupling coefficient decreases as two-dimensional effects dominate the plasmadynamics. A result for $\hat{\tau} = 3$ ($t = 36$ μs) is shown. After pulse termination, the coupling coefficient again increases as a result of energy transfer after the laser pulse ends. The final values of the coupling coefficient (10% for $\hat{\tau} = 1$ and 5% for $\hat{\tau} = 3$) are obtained by setting $t = \infty$ in Eq. (28). Shown for comparison is the 2D computer result of Boni et al. for the same conditions.[17] The two results are in good agreement except for time just before the $\hat{\tau} = 1$ point when the computer result exhibits a decrease in the coupling resulting from radiative diffusion from the leading edge of the plasma to the surface as the plasma becomes opaque.

III. Transition From an LSC to an LSD Wave Plasma

From the previous sections it can be concluded that the maximum local thermal coupling (maximum J/cm^2 delivered) occurs when a high-pressure, strongly radiating LSC wave plasma is ignited. When an LSD wave is ignited, the corresponding plasma pressure and temperature are such that the energy transfer is a smaller fraction of the incident energy (e.g., see Table 1 and Fig. 5). In order to determine the laser parameters for maximum coupling along with the

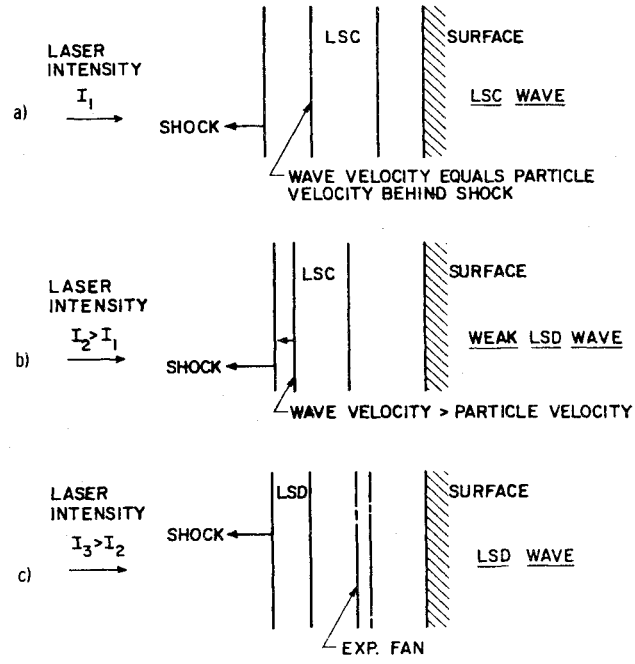

Fig. 8 Dynamics of LSC/LSD wave transition.

scaling of the coupling coefficient with laser parameters, it is necessary to describe how the the transition from the LSC wave plasma to the LSD wave plasma takes place. A schematic description of how this transition may occur is shown in Fig. 8. The top configuration (Fig. 8a), corresponding to laser intensity I_1 is similar to the LSC wave plasma shown in Fig. 2. The LSC wave propagates into the shocked air at a very low velocity; thus, the absolute wave velocity approximately equals the particle velocity behind the shock. Since the mass flow through the LSC wave is very low, the plasma temperature is high, leading to strong radiation from the plasma. The pressure throughout the region between the wall and the precursor shock is approximately constant provided the geometry remains one-dimensional. When the laser intensity is increased, corresponding to laser intensity I_2, the middle configuration (Fig. 8b) is anticipated as the transition to the LSD wave plasma begins. The LSC wave velocity is now greater than the particle velocity behind the shock since the radiative transfer and the higher temperatures behind a stronger shock result in higher LSC wave speeds. Thus, W (see Sec. II) increases. We have defined this as the "weak" LSD wave (WLSD) regime where the pressure decreases across the LSC wave. This is somewhat of a misnomer since it more closely resembles an overdriven detonation consisting of a strong shock followed by a weak deflagration wave. W continues to increase as the laser intensity is increased until the relative particle velocity behind the LSC wave becomes sonic (the Chapman-Jouquet point). The value of W, along with the associated plasma properties, when this occurs, can be calculated by examining Eqs. (2-12). In a reference frame attached to the LSC wave, the relative particle velocity behind the LSC wave is V_w. Setting $V_w^2 = \gamma p/\rho$ in Eq. (4) and equating p/p_s from Eqs. (4) and (11), we obtain an expression for W when the Chapman-Jouquet point is reached.

Table 1 "Weak" LSD wave properties

I_0, W/cm^2	P, atm	T, K
10^7	60	10,000
2×10^7	100	14,000
5×10^7	180	18,500

$$W(\text{C-J point}) = -\frac{(\gamma+1)}{2} + \frac{(\gamma_s-1)}{4}\sqrt{\left[\frac{2(\gamma+1)}{(\gamma_s-1)}\right]^2 + \frac{8\gamma}{(\gamma_s-1)}} \tag{30}$$

When $\gamma_s = 1.4$ and $\gamma = 1.2$, Eq. (30) yields $W \approx 0.1$. At this point the plasma will be designated a "weak" LSD wave plasma. The conditions behind a "weak" LSD wave can be obtained by substituting $W = 0.1$ into Eqs. (9-12). If I_p is set to equal to I_0, typical results for the plasma temperatures and pressure (using the state relation of Gilmore,[13] $h = 6.7 \times 10^{11}$ $[p(\text{atm})]^{-1/9}$ $[T(\text{eV})]^{5/3}$ ergs/g, to relate enthalpy to pressure and temperature) are shown in Table 1.

In order for W to increase further, expansion fans must form above the surface to satisfy the wall condition of zero absolute particle velocity. This is the final stage of the transition. When the intensity is I_3, the classical configuration of the LSD wave above a surface[8] is observed, as shown in the bottom schematic of Fig. 8. The absorption zone now has a velocity equal to the shock velocity; the conditions behind the absorption zone are given by classical LSD wave theory, and the surface conditions correspond to the properties behind the expansion fan.

IV. Laser Pulse Shape for Maximum Thermal Coupling

From the preceding analyses it is possible to construct the optimum laser pulse shape for maximum thermal coupling. The maximum energy transfer per unit area is obtained when a slowly propagating LSC wave plasma is ignited behind a strong precursor shock in a one-dimensional geometry. The pressure is high; the temperature is high because the absolute wave velocity approximately equals the particle velocity so the mass flow through the LSC wave is small; from Fig. 5, the radiation from the plasma is maximized under these conditions. When transition to the LSD wave plasma begins, the mass flow through the LSCW absorption zone increases, and increasing the laser intensity further simply partitions more energy into a higher mass flow. The wave propagates faster, but the energy transfer does not increase; when an LSD wave configuration is ignited, the temperature may actually be lower than for the LSC wave case since the wave is propagating at higher velocity.

The optimum laser pulse for maximum thermal coupling is shown schematically in Fig. 9. It is desirable to ignite a plasma as rapidly as possible, maintain an LSC wave plasma, and then terminate the pulse when two-dimensional effects reduce the temperature and pressure in the plasma. Therefore, the early part of the pulse consists of a spike in intensity to ignite the plasma rapidly. Ignition requirements have been specified by Musal[3] in terms of a minimum laser intensity and a minimum fluence requirement (energy/area). The minimum intensity defines the amplitude of the spike and the minimum fluence requirement defines the spike duration. Once the plasma is ignited, the intensity is reduced to a plateau intensity

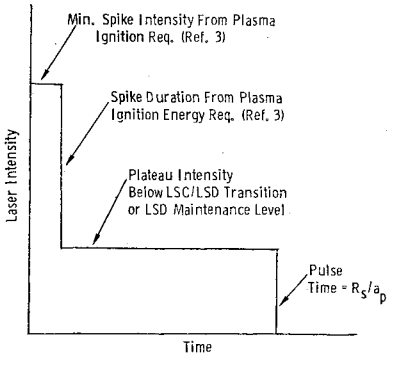

Fig. 9 laser pulse shape for maximum thermal coupling.

that sustains an LSC wave plasma. This intensity must be below the LSC/LSD transition intensity to prevent the LSD wave from forming. If an LSD wave is ignited by the spike, the intensity must also be reduced below the LSD wave maintenance level. The lower of these two intensity requirements should be chosen for the maximum plateau intensity. Two-dimensional effects begin to cool the plasma and reduce the radiative transfer when $\hat{\tau} > 1$. Therefore, for enhanced thermal coupling via radiation from the plasma, the maximum pulse time is set equal to the spot radius divided by the sound speed in the plasma.

If the pulse time is lengthened such that $\hat{\tau} \gg 1$, the plasma may expand and become sufficiently transparent that the 10.6 μ laser radiation will again reach the surface. This may lead to secondary plasma ignition and subsequent enhanced thermal coupling. Also, other mechanisms may possibly lead to increased thermal coupling in this limit. The analysis in this paper is restricted to time scales where the plasma remains opaque to the laser radiation while the pulse is on. Therefore, the model presented here may not be valid for $\hat{\tau} \gg 1$.

An example laser pulse shape for maximum thermal coupling when a 10.6 μ laser irradiates an aluminum surface can now be constructed. Prompt plasma ignition requires a minimum intensity of 10^7 W/cm^2 and a minimum delivered fluence of 1 J/cm^2, as presented in Ref. 3. Therefore, the spike must be at least 10 ns in duration if the intensity in the spike is 10^8 W/cm^2, and at least 100 ns in duration if the intensity is 10^7 W/cm^2. The intensity in the spike, however, must not be below the 10^7 W/cm^2 level. The maximum plateau intensity is the approximate intensity at which LSC/LSD wave transition begins for 10.6 μm. This intensity is estimated in the following way.

In the one-dimensional LSC wave analysis performed in Ref. 3, the radiative equilibrium assumption is utilized as $W \to 0$. As W increases, it would be expected that, when transition begins, the radiative equilibrium assumption fails. Using the radiative equilibrium assumption, we have

$$q_r = I_0/2 = \epsilon\sigma T^4 \tag{31}$$

where ϵ is the effective plasma emissivity. Specifying the plasma thickness, we can then use Eq. (31) along with Eqs. (2), and (9-11) in the limit $W \to 0$ and the Gilmore state equation to obtain W as a function of I_0. I_p is set equal to $I_0/2$ and q_l is neglected for simplicity. In the leading edge of the LSC wave, the air is heated from the temperature behind the shock to an "ignition temperature" (the temperature at which inverse Bremsstrahlung absorption becomes significant). The energy equation written between the "ignition" state and the final plasma state can be written:

$$\rho_s(V_w - u_s)(h - h_i) = I_0 - q_f - q_r \tag{32}$$

where h_i is the enthalpy corresponding to the ignition temperature T_i, and q_f is the radiation away from the plasma into the shocked air that provides the mechanism by which the LSC wave propagates. When radiative equilibrium is assumed, the left side of Eq. (32) becomes negligible and $q_f \approx q_r$. Therefore, $q_r/I_0 \approx 0.5$. With the radiative equilibrium assumption the energy equation [Eq. (2)] can be approximated by:

$$\frac{\rho_s(V_w - u_s)h}{I_0} = \frac{\rho_s u_s W h}{I_0} = 0.5 \tag{33}$$

Equation (32) can also be written as:

$$\frac{\rho_s(V_w - u_s)h}{I_0} - \frac{\rho_s(V_w - u_s)h_i}{I_0} = 1 - \frac{q_r}{I_0} - \frac{q_f}{I_0} \tag{34}$$

Therefore, when $\rho_s(V_w - u_s)h_i/I_0 = 0.5$, the radiative equilibrium assumption is valid and as I_0 increases, ρ_s $(V_w -$

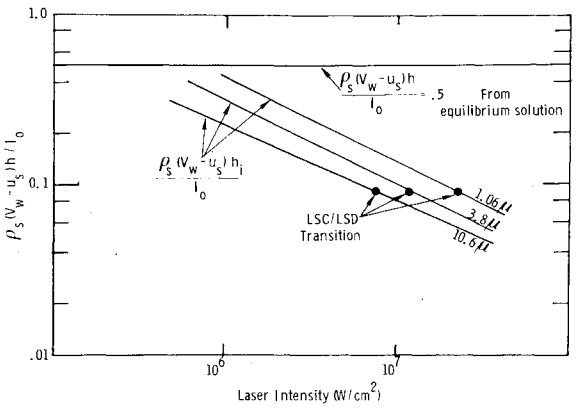

Fig. 10 Calcualtion procedure for LSC/LSD transition.

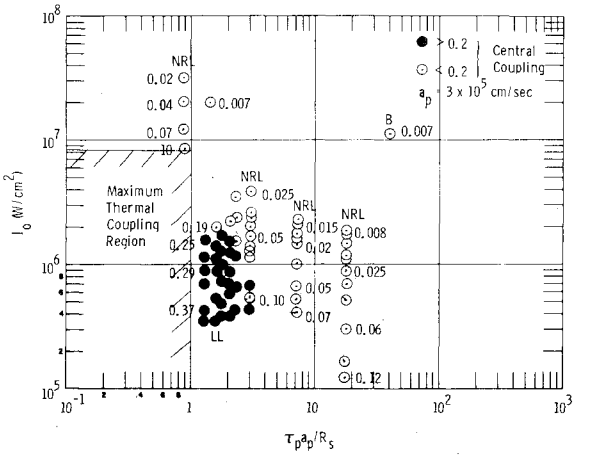

Fig. 11 Central coupling coefficient data correlation with theory concepts (10.6 μ).

$u_s)h_i/I_0$ will decrease as transition to an LSD wave plasma occurs. We use the plasma properties calculated assuming radiative equilibrium to determine $\rho_s\ (V_w-u_s)h_i/I_0$ as a function of intensity. Results are shown in Fig. 10. The ignition temperature is taken to be 14,000 K for 10.6 μm and 1 atm.[11] However, T_i is then scaled with pressure according to the inverse Bremsstrahlung absorption coefficient, because the pressure behind the precursor shock is much greater than 1 atm. Therefore, at the transition point, it was found that $T_i=0.8$ eV. From Fig. 10 it can be seen that $\rho_s\ (V_w-u_s)h_i/I_0$ (for 10.6 μm) approaches 0.5 at approximately 2×10^5 W/cm² and decreases from this value as you increase the laser intensity. At 8×10^6 W/cm², $q_r/I_0\approx0.33$ since the expression

$$\frac{\rho_s(V_w-u_s)h}{I_0}-\frac{\rho_s(V-u_s)h_i}{I_0}\rightarrow 0.44 \tag{35}$$

and q_r is set equal to q_f. This is taken as the transition point above which the idealized coupling coefficient would decrease below 33%. the LSD wave maintenance threshold is above this intensity for 1 atm ambient air. Therefore, the transition intensity of 8×10^6 W/cm² is taken to be the maximum plateau intensity. The minimum plateau intensity is the LSC wave maintenance intensity which is much less than 10^6 W/cm². Finally, the pulse time requirement of $\tau_p\leq R_s/a_p$ completes the pulse shape specification for "enhanced" thermal coupling. The plateau intensity requirements for 3.8 and 1.06 μ are also shown in Fig. 10. The inverse Bremsstrahlung absorption coefficient

$$K_\nu\sim\lambda^2 p e^{-I/kT} \tag{36}$$

where λ is the laser wavelength, I is the air ionization potential, and k is Boltzmann's constant. If ignition is defined as when the absorption coefficient approaches a constant, the "ignition temperature" scaling with wavelength and pressure becomes

$$\frac{I}{T_i}-\frac{I}{T_{i_{10.6\,\mu\ 1\ \text{atm}}}}=\ell n\left(\frac{p}{1\ \text{atm}}\right)+2\ell n\left(\frac{\lambda}{10.6\ \mu}\right)$$

Thus, the "ignition temperature" scales like the logarithm of $1/\lambda$, and the scaling of the transition intensity with wavelength is weak.

V. Data Interpretation and Comparison with Theory

There has been a substantial amount of experimental data obtained for the thermal coupling coefficient when a high-power pulsed laser irradiates an aluminum target. Many of these data are not useful for material removal assessment because the measurements are of the ratio of the total energy coupled to the total laser energy. Without a knowledge of the area over which the energy is coupled (when a plasma is ignited) nor the coupled energy/area distribution, the effectiveness of removing material with a repetitively pulsed laser cannot be determined. However, recently significant data have been obtained for the "central" coupling coefficient as defined in Sec. II. It is useful to use these data to verify the concept of an optimum laser pulse shape for maximum thermal coupling discussed in Sec. IV. This can best be done on a graph with the coordinates of plateau laser intensity vs the parameter $\tau_p a_p/R_s$. This is presented in Fig. 11 for 10.6 μm laser radiation. The plateau intensity of 8×10^6 W/cm², calculated in Sec. IV, is shown as one boundary of the cross-hatched area. The pulse time boundary of this zone is $\hat{\tau}=(\tau_p a_p/R_s)=1$. Within the cross-hatched area, maximum coupling is predicted. The data shown in Fig. 11 were obtained by the Naval Research Laboratory[18] (NRL), Lincoln Laboratory[1] (LL), and Boeing[19] (B). Since each experiment has a particular laser pulse spatial and temporal profile, an average intensity and pulse time was calculated for the equivalent square pulse. The actual values of the measured coupling coefficent are the numbers next to the data points. The solid circles correspond to coupling coefficient values greater than 20%, while the open circles indicate coupling coefficient values less than 20%. Two features are evident from these data correlation. The coupling decreases with increasing $\tau_p a_p/R_s$ at a constant laser intensity, and similarly the coupling decreases for increasing laser intensity at constant $\tau_p a_p/R_s$. This is consistent with the theory presented, since as $\tau_p a_p/R_s$ is increased, the plasmadynamics becomes more two-dimensional, and as the laser intensity is increased, LSC/LSD transition begins. At constant $\tau_p a_p/R_s$ the central coupling coefficient $\sim 1/I_0$. This may be interpreted as a saturation of the radiation from the plasma as the laser intensity is increased. When the LSC/LSD wave transition begins, no increase in temperature or pressure occurs and the larger laser energy is partitioned into higher mass flow. From Fig. 11, therefore, it can be concluded that the technique for choosing a laser pulse (Sec. IV) to maximize the thermal coupling is consistent with the existing measurements of the central coupling coefficient at 10.6 μm.

A comparison of the theoretical results obtained using Eqs. (25) and (28) (as $t\rightarrow\infty$), and $\alpha_{abs}=\beta\alpha$, with the values of β enumerated in Sec. II and the data of Fig. 11 are shown in Fig. 12. Also shown are the data of Rudder and Augustoni.[20] Since the data were taken at various intensities, the theoretical curves were calculated for two limiting intensities. Considering the simplicity of the preceding models, the comparison between theory and experiment is surprisingly good except for the Lincoln Laboratory[1] experiments (near $\hat{\tau}=1$) which resulted in coupling coefficients almost a factor of two higher than predicted. The surfaces in these experiments were

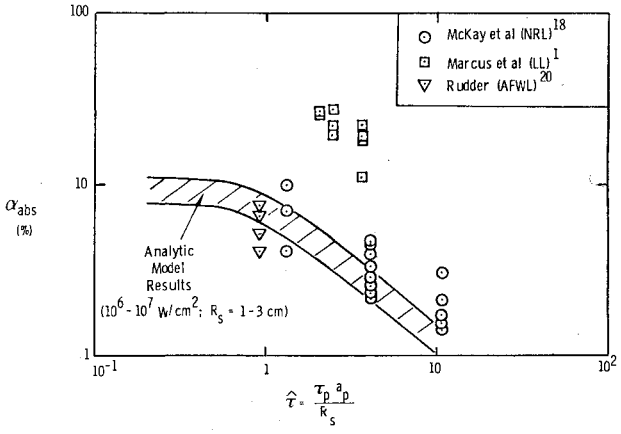

Fig. 12 Comparison of theory with 10.6 μm data.

cleaned with an abrasive material to insure a consistent plasma from pulse to pulse. The effect was to increase the number of surface protrusions and the amount of target vapor produced. Therefore, the role of target vapor in these experiments must be assessed. If it is assumed that the aluminum vapor pocket produced from a surface protrusion is $\ll 0.1$ cm in radius[6] and they are numerous, the properties of an aluminum vapor plasma can be estimated. The pockets of vapor formed from each protrusion are assumed to expand to pressure equilibrium with the surrounding air (the time scale for sound waves to propagate across the vapor pocket is much less than the vapor pocket breakdown time). If all the pockets coalesce, the resulting vapor layer has a temperature of 2750 K and a density of 10^{-4} gms/cm^3. Igniting an LSD wave in the vapor will result in a vapor plasma temperature $>30{,}000$ K and a pressure >100 atm. Although this calculation is oversimplified, under these conditions the radiative transfer from the vapor will contribute significantly to the thermal coupling into the target (see Ref. 15).

At $\hat{\tau} = 10$ the data in Fig. 12 also tend to lie above the theoretical results. Although the data scatter makes it difficult to conclude that there is a physical reason for this, it was pointed out earlier that for $\hat{\tau} \gg 1$, the model would be expected to break down because of the assumption that the laser radiation never reaches the surface after plasma ignition. There are also limited data in Ref. 5 for $\hat{\tau} \gg 1$ that show thermal coupling greater than that predicted from the intrinsic absorptivity of the aluminum.

VI. Conclusions

Based upon the theory just presented, the following conclusions can be made:

1) "Enhanced" thermal coupling can be explained in terms of the energy transfer from the plasma ignited above the reflective metal surface.

2) At just above the plasma threshold, a strongly radiating LSC wave plasma is ignited that couples thermal energy into the target very effectively.

3) When the laser intensity is increased and an LSD wave plasma forms, the energy transfer by radiation does not increase. The thermal coupling coefficient decreases dramatically. The local energy transfer (energy/area) coupled to the target may be less than 3% of the laser fluence for aluminum targets at 10.6 μm.

4) An optimum laser pulse can be designed to yield maximum thermal coupling to the target. A spike initiates the plasma rapidly and the intensity is then reduced to a level that maintains an LSC wave plasma but does not lead to formation of an LSD wave plasma. The pulse is terminated before two-dimensional effects reduce the thermal radiation from the plasma.

5) Theoretical results for the thermal coupling coefficient obtained using the plasmadynamics model of Sec. II are consistent with the limited experimental data; however, the effects of target vapor must be included when interpreting data taken with surfaces that have been abraded.

Acknowledgment

This research was sponsored jointly by the High Energy Laser Project Office (PMS-405) of the U.S. Naval Sea Systems Command and the U.S. Army High Energy Laser Systems Project Office under Contracts N00014-74-C-0207, N00173-76-C-0216, and DAAK40-76-C-1289. The contract monitors were J. T. Schriempf and R. Sepucha.

References

[1] Marcus, S., Lowder, J. E., and Mooney, D. L., "Large-Spot Thermal Coupling of CO_2 Laser Radiation to Metallic Surfaces," *Journal of Applied Physics*, Vol. 47, July 1976, p. 2966.

[2] Raizer, Y. P., "Subsonic Propagation of a Light Spark and Threshold Conditions for the Maintenance of a Plasma by Radiation," *Soviet Physics-JETP*, Vol. 31, No. 6, Dec. 1970.

[3] Boni, A. A., Su, F. Y., Thomas, P. D., and Musal, H. M., "Theoretical Study of Laser-Target Interactions," Mid-Term Tech. Rept. SAI 76-722-LJ, Science Applications, Inc., LaJolla, Calif., Aug. 1976.

[4] Pirri, A. N., "Analytic Solutions for Laser-Supported Combustion Wave Ignition Above Surfaces," AIAA Paper 76-23, Washington, D.C., Jan. 1976.

[5] Reilly, D. A. and Rostler, P. S., "Pre-Breakdown Laser Target Vaporization and Enhanced Thermal Coupling, Final Technical Report," Avco Everett Research Laboratory Report for Contract N00014-73-C-0457, Aug. 1974.

[6] Walters, C. T., Barnes, R. H., and Beverly III, R. E., "An Investigation of Mechanisms of Initiation of Laser-Supported Absorption (LSA) Waves," Final Report for DAAH01-73-C-0776, Battelle Columbus Laboratories, Columbus, Ohio, Sept. 1975.

[7] Raizer, Y. P., "Heating of a Gas by a Powerful Light Pulse," *Soviet Physics-JETP*, Vol. 21, 1965, p. 1009.

[8] Pirri, A. N., "Theory for Momentum Transfer to a Surface with a High-Power Laser," *The Physics of Fluids*, Vol. 16, Sept. 1973, p. 1435.

[9] Pirri, A. N., Kemp, N. H., Root, R. G., and Wu, P. K. S., "Theoretical Laser Effects Studies," Final Report, PSI TR-89, Physical Sciences Inc., Woburn, Mass., Feb. 1977.

[10] Su, F. Y. and Boni, A. A., "Non-Linear Model of Laser-Supported Deflagration Waves," *The Physics of Fluids*, Vol. 19, July 1976, p. 960.

[11] Jackson, J. P. and Nielsen, P. E., "Role of Radiative Transport in the Propagation of Laser-Supported Combustion Waves," *AIAA Journal*, Vol. 12, Nov. 1974, p. 1498.

[12] Johnston, R. R., Platas, O. R., and Tannenwald, L. M., "Atomic Line Transitions and Radiation from High Temperature Air," Rept. N-3L-70-1, Lockheed Palo Alto Research Laboratory, Palo Alto, Calif., July 1970.

[13] Gilmore, F. R., "Equilibrium Composition and Thermodynamic Properties of Air to 24,000 K," RM-1543, The Rand Corp., Santa Monica, Calif., Aug. 1955.

[14] Jackson, J. P. and Jumper, E. J., "Mechanisms of Enhanced Coupling by a Pulsed Laser," Laser Division Digest, AFWL-TR-75-229, Air Force Weapons Laboratory, Oct. 1975, p. 172.

[15] Pirri, A. N., Root, R. G., and Wu, P. K. S., "Plasma Energy Transfer to Metal Surfaces Irradiated by Pulsed Lasers," Paper 77-658, June 1977; also *AIAA Journal*, to be published.

[16] Wilson, K. H. and Greif, R., "Radiation Transport in Atomic Plasmas," *Journal of Quantitative Spectroscopy and Radiative Transfer*, Vol. 8, 1968, pp. 1061-1086.

[17] Boni, A. A., Su, F. Y., Thomas, P. D., and Musal, H. M., "Theoretical Study of Laser-Target Interactions," Final Tech. Rept. SAI 77-567 LJ, Science Applications Inc., LaJolla, Calif., May 1977.

[18] McKay, J. A., Stegman, R. L., and Schriempf, J. T., "Thermal Effects of Pulsed Laser Irradiation," 2nd DoD High Energy Laser Conference Proceedings, Col. Springs, Col., Nov. 1976.

[19] Hall, R. B., Wei, P. S. P., and Maher, W. E., "Laser Beam Target Interaction-Vol. II, Laser Effects at 10.6 μ," AFWL-TR-75-342, Vol. II, Air Force Weapons Laboratory Rept., July 1976.

[20] Rudder, R. R. and Augustoni, A. L., "Thermal Deposition Experiments with Microsecond Duration CO_2 Laser Radiation," Laser Digest-Summer 1975, AFWL-TR-75-229, Air Force Weapons Laboratory, Kirtland Air Force Base, N. Mex., Oct. 1975.